^{89}Zr-Bevacizumab PET Visualizes Disease Manifestations in Patients with von Hippel–Lindau Disease

Sjoukje F. Oosting*[1], Sophie J. van Asselt*[1,2], Adrienne H. Brouwers[3], Alfons H.H. Bongaerts†[1,4], Julia D.J. Steinberg[5], Johan R. de Jong[3], Marjolijn N. Lub-de Hooge[3,6], Anouk N.A. van der Horst-Schrivers[2], Annemiek M.E. Walenkamp[1], Eelco W. Hoving[7], Wim J. Sluiter[2], Bernard A. Zonnenberg[8], Elisabeth G.E. de Vries[1], and Thera P. Links[2]

[1]Department of Medical Oncology, University of Groningen, University Medical Center Groningen, Groningen, The Netherlands; [2]Department of Endocrinology, University of Groningen, University Medical Center Groningen, Groningen, The Netherlands; [3]Department of Nuclear Medicine and Molecular Imaging, University of Groningen, University Medical Center Groningen, Groningen, The Netherlands; [4]Department of Radiology, University of Groningen, University Medical Center Groningen, Groningen, The Netherlands; [5]Department of Radiology, Martini Hospital Groningen, Groningen, The Netherlands; [6]Hospital and Clinical Pharmacy, University of Groningen, University Medical Center Groningen, Groningen, The Netherlands; [7]Department of Neurosurgery, University of Groningen, University Medical Center Groningen, Groningen, The Netherlands; and [8]Department of Internal Medicine, University of Utrecht, University Medical Center Utrecht, Utrecht, The Netherlands

Patients with von Hippel–Lindau disease (VHL) are at risk to develop multiple tumors. The growth of lesions is unpredictable, and regular surveillance is critical for early treatment to control local damage. Vascular endothelial growth factor A (VEGF-A) produced locally is supposed to play an important role in development of disease manifestations and is a target for antiangiogenic therapy with the monoclonal antibody bevacizumab. We aimed to assess whether VHL manifestations can be visualized with ^{89}Zr-bevacizumab PET and to explore whether ^{89}Zr-bevacizumab PET can differentiate progressive from nonprogressive lesions. **Methods:** VHL patients with at least 1 measurable hemangioblastoma were eligible. ^{89}Zr-bevacizumab (37 MBq) was administered intravenously 4 d before the scan. Maximum standardized uptake values were calculated. PET scans were fused with routine MRI of the central nervous system and abdominal MRI or CT. Progressive lesions were defined as new lesions, lesions that became symptomatic, and lesions $\geq$ 10 mm that increased $\geq$ 10% and $\geq$ 4 mm on repeated anatomic imaging within 12 mo. **Results:** Twenty-two patients were enrolled. At baseline, anatomic imaging showed 311 lesions. ^{89}Zr-bevacizumab PET visualized 59 VHL manifestations, 0–17 per patient. The median of maximum standardized uptake values was 8.5 (range, 1.3–35.8). The detection rate for lesions $\geq$ 10 mm was 30.8%. Seven additional hotspots without substrate on baseline anatomic imaging were found; 2 were also detected with anatomic imaging during follow-up. Nine of 25 progressive lesions were visible on PET and 27 of 175 nonprogressive lesions, corresponding to a positive predictive value of 25% and a negative predictive value of 90%. SUV_{max} was similar in progressive and nonprogressive lesions (median, 4.8; range, 0.9–8.9 vs. median, 6.7; range, 1.3–35.8, $P = 0.14$). **Conclusion:** VHL manifestations can be visualized with ^{89}Zr-bevacizumab PET with a striking heterogeneity in tracer accumulation. ^{89}Zr-bevacizumab uptake does not predict progression within 12 mo. In one third of the lesions, the drug target VEGF is available and accessible. ^{89}Zr-bevacizumab PET might offer a tool to select VHL patients for anti-VEGF therapy.

Key Words: von Hippel-Lindau disease; hemangioblastoma; positron emission tomography; vascular endothelial growth factor; bevacizumab

J Nucl Med 2016; 57:1244–1250
DOI: 10.2967/jnumed.115.167643

Von Hippel–Lindau (VHL) disease is an autosomal-dominant inherited tumor syndrome caused by an inactivating germline mutation in the *VHL* gene, located on chromosome 3p25. The estimated prevalence is 2–3 per 100,000 (*1,2*). Inactivation or loss of the wild-type *VHL* allele results in disease manifestations. Lack of functional VHL protein induces intracellular accumulation of the transcription factor hypoxia-inducible factor 1α, activating cellular survival strategies for hypoxic circumstances by angiogenesis via proangiogenic growth factors including vascular endothelial growth factor A (VEGF-A). The main VHL disease manifestations are hemangioblastomas, retinal angiomas, renal cell carcinomas, pancreatic neuroendocrine tumors, pheochromocytomas, middle ear endolymphatic sac tumors, and cysts in the kidneys, pancreas, epididymis, and broad ligament. *VHL* mutation carriers often develop multiple disease manifestations that can severely affect quality of life. Moreover, patients with VHL disease have a shorter life expectancy (*3*).

Guidelines for screening and surveillance of existing lesions advise frequent imaging, ocular examination, and blood and urine examination (*4,5*). There is no validated tool that predicts the progression of disease manifestations. Hemangioblastomas are often dormant for years but can suddenly start growing; 72% grow in a saltatory pattern (*6,7*). Hemangioblastoma growth is associated with location in the brain stem and cerebellum, male sex, and a cystic component (*6*). Local concentrations of growth factor VEGF-A may provide predictive information on biologic behavior of VHL-associated lesions. Early identification of progressive lesions allows timely local treatment. Furthermore, different drugs

Received Sep. 30, 2015; revision accepted Jan. 15, 2016.
For correspondence or reprints contact: Thera P. Links, Endocrinology Department, AA31, University Medical Center Groningen, P.O. Box 30,001, 9700RB Groningen, The Netherlands.
E-mail: t.p.links@umcg.nl
*Contributed equally to this work.
†Deceased.
Published online May 12, 2016.

are available to target the VEGF-A pathway at the growth factor level as well as at the receptor level. We developed the PET tracer ^{89}Zr-bevacizumab that binds VEGF-A and enables noninvasive whole-body imaging and quantification. In patients with sporadic metastatic renal cell carcinoma, ^{89}Zr-bevacizumab PET visualized tumor lesions including brain metastases, illustrating that the radioactive tracer can cross the blood–brain barrier (*8*).

The aim of the present feasibility study was to assess whether VHL-associated lesions can be visualized with ^{89}Zr-bevacizumab PET and whether ^{89}Zr-bevacizumab PET can differentiate progressive from nonprogressive lesions.

MATERIALS AND METHODS

Patients

Patients were recruited from the University Medical Centers in Groningen and Utrecht. Eligibility criteria included genetically proven VHL disease or clinically proven VHL disease (*4*), age ≥ 18 y, participation in a surveillance program, and at least 1 measurable lesion located in the central nervous system (CNS). Pregnant patients were excluded. Treatment for VHL disease manifestations was recorded up to 12 mo after ^{89}Zr-bevacizumab PET imaging. The study was approved by the institutional review board (http://www.clinicaltrials.gov NCT00970970). All patients gave written informed consent.

^{89}Zr-Bevacizumab PET

PET scans were obtained at the University Medical Center Groningen. Conjugation and labeling of bevacizumab (25 mg/mL; Roche) with ^{89}Zr was performed as described (*9*). Whole-body PET images were acquired on a Biograph mCT (PET/CT 64 slices; Siemens) scanner from the upper legs to head in 6–8 bed positions of 5-min acquisition time each. Administration of 37 MBq of ^{89}Zr provides a resolution of approximately 10 mm on PET and reconstruction settings used. The first 3 patients underwent PET scans at 1 h, 2 d, and 4 d after intravenous administration of ^{89}Zr-bevacizumab (37 MBq, protein dose of 5 mg). The optimal scan timing with the highest lesion-to-background ratio was day 4. The next patients underwent PET scanning 4 d after ^{89}Zr-bevacizumab administration.

Standard Screening and Surveillance

Patients underwent MRI of the CNS within 6 wk before ^{89}Zr-bevacizumab PET and abdominal CT or MRI within 3 mo before or after ^{89}Zr-bevacizumab PET. Follow-up anatomic imaging was performed within 12 mo of initial surveillance. MR images were acquired with a 1.5-T scanner in T1- and T2-weighted sequences, with and without intravenous administration of a gadolinium-containing contrast agent. The reconstruction interval varied between 1 and 5 mm for CNS and between 1.5 and 5 mm for abdominal imaging. CT scans were acquired with a multidetector scanner, before and after intravenous administration of an iodine-containing contrast agent, with a maximum slice thickness of 5.0 mm. CNS and abdominal imaging were centrally reviewed by *2* radiologists. Morphologic aspect (cystic, solid, mixed) and maximal lesion diameters were recorded.

Imaging Analysis

The ^{89}Zr-bevacizumab PET scans were fused with baseline MRI or CT scans using SyngoMMWP VE50A software (Siemens AG) to verify substrate for hot spots. Tracer uptake was quantified by calculating SUV_{mean} and SUV_{max} for PET-positive VHL-associated lesions and healthy organs with AMIDE Medical Image Data Examiner software (version 0.9.1; Stanford University) by drawing 3-dimensional regions of interest (*10*). Quantification of ^{89}Zr-bevacizumab distribution revealed a strong correlation between SUV_{max} and SUV_{mean} for normal organs ($r = 0.99$, $P < 0.01$) and VHL disease manifestations ($r = 0.97$, $P < 0.01$, Supplemental Fig. 1 [supplemental materials are available at http://jnm.snmjournals.org]). SUV_{max} is less operator dependent and therefore reported. Given the resolution of ^{89}Zr-bevacizumab PET, we did a subanalysis of lesions ≥ 10 mm.

For all lesions visualized on baseline CT/MRI except simple renal and pancreatic cysts, progression was recorded and compared with ^{89}Zr-bevacizumab PET. Because a definition for progression of VHL manifestations and information on variability of measurements on repeated imaging are lacking, we took a conservative approach based on variability of lung tumor CT measurements (*11*). We considered lesions with a longest diameter of ≥ 10 mm that increased ≥ 10% and an absolute growth of ≥ 4 mm progressive, as well as new lesions visualized on the follow-up scan and lesions that became symptomatic.

TABLE 1
Patient Characteristics

Characteristic	Total population (n = 22)	
	n	%
Sex		
Male	13	59
Female	9	41
Age (y)		
Median	42	
Range	23–66	
Mutation		
c.-89-?_c.297+?del	10	45
c.500G > A	5	23
c.509T > A	3	14
c.490C > T	1	5
c.340 + 1G > A	1	5
c.241C > T	1	5
IVS1-59del46 (unclassified variant)	1	5
History		
Hemangioblastoma	22	100
Retinal angioma	15	68
Renal cell carcinoma*	8	36
Pancreatic neuro-endocrine tumor	5	23
Pheochromocytoma	4	18
Prior treatment (no. of patients/procedures)		
Craniotomy	12/28	55
Spinal cord hemangioblastoma embolization	2/2	9
Retinal laser/cryotherapy	14/19	64
(Partial) nephrectomy	8/13	36
Adrenalectomy	4/7	18
(Partial) pancreatectomy	2/2	9

*One patient had a renal cell carcinoma recurrence on regular surveillance at time written informed consent was given and study imaging was already planned. This patient was motivated for study participation.

TABLE 2
VHL Disease Manifestations on Routine Imaging and on ^{89}Zr-Bevacizumab PET Per Patient

Patient no.	Sex	Mutation*	Age (y)	VHL manifestations† at baseline anatomic imaging (*n*)	MRI/CT lesions ≥ 10 mm (*n*)	PET lesions (*n*)	SUV_{max} range
1	Male	1	57	CNS (5), pancreas (2)	2	2	4.8–6.0
2	Female	1	23	CNS (1)	1	0	
3	Male	1	31	CNS (8), kidney (1), epididymis‡ (1)	3	1	12.2
4	Male	4	61	CNS (4), kidney (8), pancreas (1)	10	7	6.6–27.6
5	Female	2	61	CNS (13), kidney (3), pancreas (1)	9	8	2.4–28.3
6	Male	1	62	CNS (3), pancreas (2)	3	1	6.7
7	Female	1	36	CNS (19), pancreas (2)	3	3	1.3–2.8
8	Female	1	29	CNS (10), pancreas (1)	2	1	1.4
9	Male	7	33	CNS (2), pancreas (2)	1	1	4.3
10	Female	2	48	CNS (9), kidney (4), pancreas (1)	5	1	1.6
11	Female	1	29	CNS (7)	1	1	1.6
12	Female	2	38	CNS (4), pancreas (1), adrenal gland (1)	1	2	4.1–6.4
13	Male	1	63	CNS (4), kidney (4), pancreas (1)	3	0	
14	Female	3	46	CNS (1), pancreas (1)	1	0	
15	Female	1	60	CNS (1), pancreas (1), liver (100), bone¶ (1)	81	18	5.7–15.4
16	Male	2	26	CNS (3)	1	0	
17	Male	5	32	CNS (8), kidney (2), pancreas (1)	3	3	4.3–35.8
18	Male	1	31	CNS (7)	0	0	
19	Male	3	50	CNS (55), epididymis‡ (1)	5	7	2.7–9.0
20	Male	2	46	CNS (1)	1	0	
21	Male	3	66	CNS (4)	2	2	3.4–5.7
22	Male	6	35	CNS (1), kidney (1)	1	1	26.6

*Mutation, 1 = c.-89-?_c.297+?del, 2 = c.490C > T, 3 = c.500G > A, 4 = c.509T > A, 5 = c.340 + 1G > A, 6 = c.241C > T, 7 = IVS1–59del46 (unclassified variant).
†Excluding simple cysts.
‡Demonstrated on ultrasound.
¶Demonstrated on ^{11}C-hydroxytryptophan PET and MRI.

Plasma VEGF-A

Before each ^{89}Zr-bevacizumab administration, a blood sample was obtained by peripheral vena puncture, using a tourniquet. Blood was collected in sterile 10-mL ethylenediaminetetraacetic acid tubes. Within 30 min of collection, ethylenediaminetetraacetic acid blood was centrifuged at 120*g* for 30 min at 4°C. After collection of 0.25 mL of platelet-rich plasma, the leftover was centrifuged again at 2,500*g* for 10 min at room temperature to obtain platelet-poor plasma. Plasma sample aliquots were stored at −80°C. VEGF-A was determined in platelet-poor plasma in duplicate using the Quantikine enzyme-linked immunosorbent assay kit (R&D Systems) according to the manufacturer's instructions. The mean of the duplicates was used for calculations. Plasma VEGF-A was compared with ^{89}Zr-bevacizumab PET results.

Statistical Analysis

The primary endpoint was the detection rate of ^{89}Zr-bevacizumab PET for VHL disease manifestations. Spearman rank correlations served to calculate correlations. For comparison of unpaired data the Mann–Whitney test was used, and for paired data the Wilcoxon signed-rank test was used. Differences in PET positivity rate between progressive and nonprogressive lesions were tested using the Fisher exact test. A *P* value of less than 0.05 was considered statistically significant. Analyses were performed with SPSS (version 20; IBM) and GraphPad Prism (version 5.00; GraphPad Prism Inc.).

RESULTS

Patient Characteristics

Between November 2009 and April 2012, 13 male and 9 female patients were included (median age, 42 y; range, 23–66 y) (patient characteristics are shown in Table 1).

Routine Anatomic Imaging

Three hundred eleven VHL disease manifestations other than simple renal and pancreatic cysts were identified on baseline MRI and CT, with a median of 7 per patient (range, 1–102) (Tables 2 and 3). In total, 139 lesions were ≥ 10 mm. Furthermore, 130 simple cysts ≥ 5 mm were detected in the kidneys (range, 0–46 per patient) and 126 in the pancreas (range, 0–30).

^{89}Zr-Bevacizumab PET

^{89}Zr-bevacizumab PET visualized 59 VHL disease manifestations, 0–17 per patient (median, 1) (Fig. 1; Tables 2 and 3). Fifty of these 59 PET-positive VHL lesions had a solid, 6 a cystic, and 2 a mixed appearance on anatomic imaging, and 1 lesion could not

TABLE 3
VHL Disease Manifestations* on Routine Imaging and on ^{89}Zr-Bevacizumab PET Per Organ

Localization	MRI/CT lesions		PET-positive lesions (*n*)	SUV_{max}	
	n	No. of ≥10 mm		Median	Range
Brain					
Cerebellum	116	15	19	4.8	1.3–8.9
Other	4	1	1	6.1	
Spine	49	12	3	4.1	3.6–6.7
Optical nerve	1	1	1	2.4	
Kidney	23	19	12	22.2	6.6–35.8
Pancreas	17	11	3	6.0	4.3–10.3
Adrenal gland	1	0	1	6.4	
Liver†	100	80	16	9.7	8.5–15.4
Epididymis‡			2	10.6	9.0–12.2
Bone¶			1	5.7	

*Not including simple cysts.
†Liver metastases of pancreatic neuroendocrine tumor.
‡Ultrasound-confirmed cystadenomas.
¶Pelvic bone metastasis of pancreas neuroendocrine tumor ^{11}C-5-hydroxytryptophan PET and MRI confirmed.

be classified. No ^{89}Zr-bevacizumab accumulation in simple renal and pancreatic cysts was demonstrated; 33 simple renal cysts appeared as cold spots.

The PET scan demonstrated 7 additional hot spots in 5 different organs without substrate on anatomic imaging. Two lesions (cerebellum, adrenal gland) were detected during follow-up on anatomic imaging.

Overall, 44 of 139 VHL disease manifestations ≥ 10 mm (30.8%) were identified on ^{89}Zr-bevacizumab PET. The detection rate of hemangioblastomas ≥ 10 mm was 16 of 29 (55%). Figure 2 shows SUV_{max} and the proportion of PET-positive lesions ≥ 10 mm for the different germline mutations.

Normal-organ distribution of ^{89}Zr-bevacizumab was similar as described earlier (Fig. 3A) (*8,12*). Median SUV_{max} of VHL disease manifestations was 8.5 (range, 1.3–35.8), with higher tracer uptake in kidney lesions (n = 12; median SUV_{max}, 22.2; range, 6.6–35.8) than in CNS lesions (n = 24; median SUV_{max}, 4.5; range, 1.3–8.9; $P < 0.0001$; Fig. 3B). However, because of the low normal-organ background in the CNS, the lesion-to-background ratio (median, 8.6; range, 1.9–25.3) was excellent for hemangioblastomas and even higher than for kidney lesions (median, 5.0; range, 2.0–11.5; $P = 0.049$).

Progressive Lesions

Repeated abdominal imaging was available in 19 patients at a median of 349 d after baseline (range, 196–642 d); repeated CNS imaging was available in 20 patients at a median of 319 d after baseline (range, 90–540 d). Out of 200 evaluable lesions, 25 were progressive (21 hemangioblastomas and 4 renal cell carcinomas).

^{89}Zr-bevacizumab PET visualized 9 of 25 (36%) progressive lesions and 27 of 175 nonprogressive lesions (15%), resulting in a positive predictive value of 0.25 (95% confidence interval, 0.11–0.39) and a negative predictive value of 0.90 (95% confidence interval, 0.86–0.95). The detection rate of ^{89}Zr-bevacizumab PET was significantly higher for progressive lesions than nonprogressive lesions ($P = 0.022$). However, progressive and nonprogressive lesions had a similar SUV_{max} (median, 4.8; range, 0.9–8.9, vs. median, 6.7; range, 1.3–35.8; $P = 0.14$). When this analysis was limited to hemangioblastomas, again a significantly higher PET detection rate for progressive (9/21 [43%]) than nonprogressive hemangioblastomas (15/148 [10%]) was found ($P = 0.001$). To explore whether the difference in detection rate could be explained by a difference in size between progressive and nonprogressive lesions, we further limited the analysis to hemangioblastomas ≥ 10 mm and found no difference in detection rate ($P = 0.71$).

Treatment

In the first year of follow-up, 8 patients were actively treated for VHL disease manifestations, and in 6 surveillance was intensified (Supplemental Table 1). Two patients received bevacizumab treatment. These patients are described in more detail in the supplemental data.

Plasma VEGF-A

Baseline plasma VEGF-A levels were available for all and follow-up levels for 14 of 22 patients. Median plasma VEGF-A was 23.9 pg/mL (range, undetectable–123.0) at baseline and 32.1 pg/mL (range, undetectable–259.7) at follow-up. No correlation was found between baseline plasma VEGF-A and the total number of VHL disease manifestations, the number of PET-positive lesions, SUV_{max}, or mean SUV_{max}. Furthermore, baseline and delta plasma VEGF-A did not differ between patients with progressive lesions and patients without progressive lesions.

DISCUSSION

To our knowledge, this is the first study demonstrating that VHL disease manifestations can be visualized with ^{89}Zr-bevacizumab

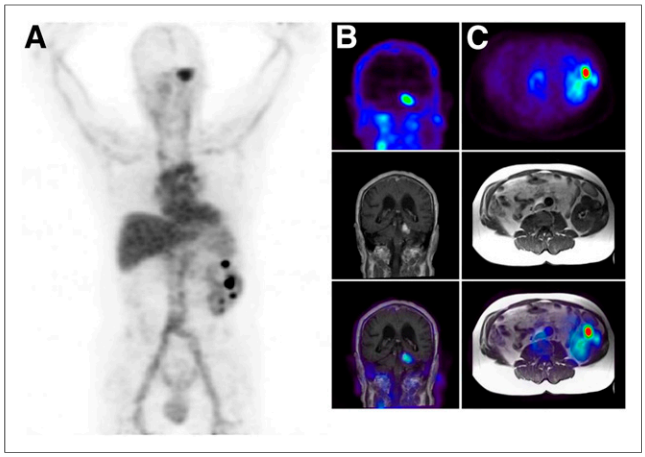

FIGURE 1. (A) ^{89}Zr-bevacizumab PET scan (maximum-intensity projection) of patient 4, demonstrating normal antibody distribution with tracer uptake in blood pool and liver as well as uptake in a hemangioblastoma in cerebellum (SUV_{max}, 8.3) and in 6 solid kidney lesions (SUV_{max}, 6.6–27.6). (B) Hemangioblastoma visualized on coronal ^{89}Zr-bevacizumab PET, MR, and fusion images (top, middle, and bottom, respectively). (C) Kidney lesion visualized on transversal ^{89}Zr-bevacizumab PET, MR, and fusion images (top, middle, and bottom, respectively).

PET. The detection rate for lesions ≥ 10 mm was 30.8%. Despite the monogenetic pathogenesis, profound heterogeneity in tracer uptake by the lesions between and within patients was demonstrated, reflected by the finding of PET-positive and -negative lesions and by the range of SUV_{max}. ^{89}Zr-bevacizumab PET did not identify lesions that progressed within the next year, nor did plasma VEGF-A levels.

Abundant VEGF expression has been demonstrated by in situ hybridization and immunohistochemistry in a variety of VHL-associated lesions (*13–18*). In contrast, VEGF messenger RNA was not detectable in normal brain (*16*) and was 3–13 times lower in normal kidney than in renal cell carcinoma (*13*). This corresponds with our imaging data that show virtually no ^{89}Zr-bevacizumab accumulation in normal brain, intermediate uptake in normal kidney, and high uptake compared with normal surrounding tissue in one third of disease manifestations. The lesion detection rate was lower than in previous studies with ^{89}Zr-bevacizumab PET in breast cancer and sporadic renal cell carcinoma patients but higher than in patients with neuroendocrine tumors (*8,9,12*). This may well represent different biology in relation to VEGF-A between these neoplasms. In the present study, there were 3 of 11 pancreatic lesions, which are probably neuroendocrine tumors, PET-positive. In addition, in a single patient only 16 of 80 liver metastases of a pancreatic neuroendocrine tumor were visible on PET. This is in line with our previous study in neuroendocrine tumor patients and highly influences the overall detection rate in the current study. Of the CNS lesions, 16 of 29 (55%) were PET-positive, which—although they are likely nonmalignant—closely resembles the detection rate we found for metastatic renal cell carcinoma. Interestingly, median SUV_{max} was numerically the highest in the current study, followed by the study in renal cell carcinoma, which is also characterized by loss of VHL and high VEGF-A expression. Median SUV_{max} was lowest in the primary breast cancer study (*9*), underscoring that these type of PET scans are more of value for characterization of lesions than in general for detection of lesions.

Accumulation of a radiolabeled antibody not only is determined by expression of the target, but also can be affected by perfusion and permeability of blood vessels, tumor interstitial pressure, and anatomic location (*19*). A small MRI study showed hyperperfusion and edema in hemangioblastomas, suggesting that vascular characteristics are not a likely cause of limited or no ^{89}Zr-bevacizumab accumulation (*20*). CT in 66 sporadic clear cell renal cancer patients demonstrated lower blood flow, blood volume, and permeability surface area in primary tumors compared with normal renal cortex but with large SD, indicating heterogeneity (*21*). These perfusion parameters were correlated with microvessel density but not with VEGF staining. Future studies combining perfusion imaging with ^{89}Zr-bevacizumab PET would enable determination of the role of vascular characteristics on antibody distribution.

In the present study, we did not perform biopsies to correlate imaging results with tissue VEGF-A concentration. However, in 9 melanoma patients and 23 breast cancer patients, radiolabeled bevacizumab uptake in the tumor correlated with tumor VEGF-A measurement by immunohistochemistry and enzyme-linked immunosorbent assay, respectively (*9,22*).

Heterogeneity in VEGF-A concentration in VHL manifestations between and within patients might be explained by different germline and second-hit mutations, resulting in variable preservation of the ability to degrade hypoxia-inducible factor 1α (*23*). The numbers of lesions in this study are too small to draw conclusions, but the results do not suggest important differences in the rate of PET-positive lesions or in SUV_{max} for different germline mutations.

In addition to being hypoxia-inducible-factor-dependent, VHL protein also has hypoxia-inducible-factor-independent functions such as stabilization of microtubules, regulation of apoptosis, regulation of extracellular matrix assembly, maintenance of primary cilium (*23*), and control of fibroblast growth factor receptor signaling (*24*). Loss of hypoxia-inducible-factor-independent functions probably contributes to the development of disease manifestations, including angiogenesis. In-depth genomic analysis of 4 synchronous renal cell carcinomas in a patient with VHL disease demonstrated different additional mutations per tumor (*25*). Therefore, intrapatient heterogeneity

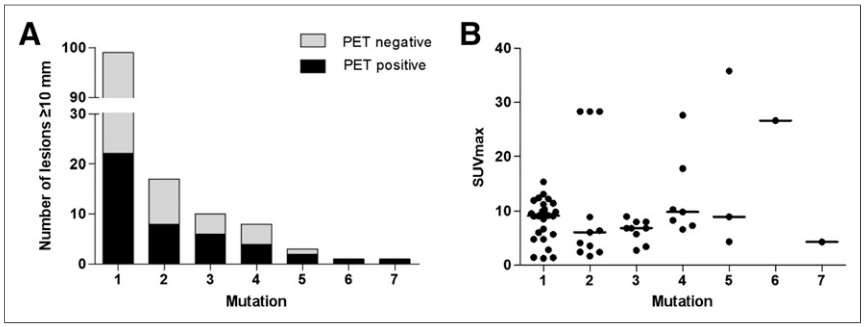

FIGURE 2. Number of PET-positive VHL disease manifestations ≥ 10 mm according to germline mutation (A) and SUV_{max} (B): 1 = c.-89-?_c.297+?del, 2 = c.500G > A, 3 = c.490C > T, 4 = c.509T > A, 5 = c.340 + 1G > A, 6 = c.241C > T, 7 = IVS1-59del46.

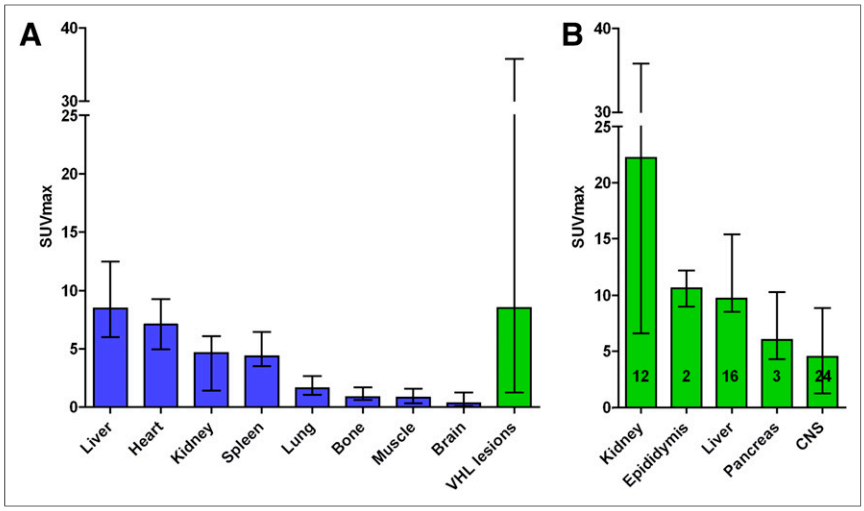

FIGURE 3. Quantification (median with range) of ^{89}Zr-bevacizumab distribution in 22 patients with VHL disease in normal organs and 59 disease manifestations (A) and in VHL disease manifestations according to localization (B).

in ^{89}Zr-bevacizumab uptake might reflect genomic heterogeneity. Whether additional mutations and mutational heterogeneity are prevalent in hemangioblastomas in VHL disease is unknown. However, sporadic hemangioblastomas are characterized by a low somatic mutation rate with exception of the *VHL* gene (*26*).

We found no difference in ^{89}Zr-bevacizumab accumulation between progressive and nonprogressive disease manifestations $\geq$ 10 mm. This contrasts with a small study in 3 VHL patients in which the highest VEGF messenger RNA level was found in the patient with the most active disease (*27*). Moreover, in 50 patients with sporadic clear cell renal cell carcinoma who underwent nephrectomy, cytoplasmic VEGF expression correlated with tumor progression and grade (*28*).

Simple cysts in kidneys and pancreatic glands did not take up ^{89}Zr-bevacizumab. Higher VEGF concentrations were detected in the fluid of 2 renal cysts than in serum of 1 VHL patient (*29*). Cyst formation may, however, be more dependent on loss of maintenance of the primary cilium than on activation of the VEGF pathway (*30*).

We did not find a relation between plasma VEGF-A levels and ^{89}Zr-bevacizumab PET imaging results. Also the number of lesions and presence of symptomatic or growing lesions were not related with plasma VEGF-A. This is in line with earlier data (*29*) and may be explained by different VEGF-A splice variants in the circulation compared with the microenvironment of disease manifestations. The small variants, consisting of 121 and 165 amino acids ($VEGF_{121}$ and $VEGF_{165}$), are freely diffusible whereas the large variants $VEGF_{189}$ and $VEGF_{206}$ are bound to the extracellular matrix (*31*). Imaging with ^{89}Zr-bevacizumab, binding to all splice variants potentially better reflects biology of disease manifestations than circulating VEGF-A.

VHL patients receive local treatment for symptomatic disease manifestations and lesions that pose a threat to functioning or have metastatic potential. There is no evidence-based systemic therapy available, but case reports and small studies have been reported for antiangiogenic treatment with bevacizumab (*32–34*), thalidomide (*35,36*), and the tyrosine kinase inhibitors semaxanib (*37–41*) and pazopanib (*42*). Study results for vatalanib and for bevacizumab are awaited (www.clinicaltrials.gov identifiers NTC00052013 and NTC01015300). Antiangiogenic therapy has resulted in improvement of symptoms and disease stabilization but rarely induces volume responses in hemangioblastomas. We treated 2 patients with bevacizumab plus interferon-α after participation in this study. One patient, who received bevacizumab plus interferon-α for metastatic renal cell carcinoma and hardly showed ^{89}Zr-bevacizumab accumulation in the tumor, did not respond and died of rapidly progressive disease after 2 mo. The other patient was treated for multiple progressive unresectable hemangioblastomas with intense uptake on the ^{89}Zr-bevacizumab PET scan. She experienced prolonged symptomatic improvement and a decrease in hemangioblastoma size. These cases suggest that ^{89}Zr-bevacizumab PET might offer a tool to select patients for anti-VEGF therapy, but this needs further evaluation in future studies.

CONCLUSION

^{89}Zr-bevacizumab PET can visualize different VHL disease manifestations but does not predict the behavior of a lesion. Striking heterogeneity between and within patients was found, reflecting different biology. Future studies are needed to assess whether ^{89}Zr-bevacizumab PET can predict sensitivity to antiangiogenic treatment.

DISCLOSURE

The costs of publication of this article were defrayed in part by the payment of page charges. Therefore, and solely to indicate this fact, this article is hereby marked "advertisement" in accordance with 18 USC section 1734. This study was supported by a grant of the American VHL Family Alliance. No other potential conflict of interest relevant to this article was reported.

ACKNOWLEDGMENT

We are grateful to Dr. Ronald van Rheenen for his help with the supplemental videos.

REFERENCES

1. Maher ER, Iselius L, Yates JR, et al. Von Hippel-Lindau disease: a genetic study. *J Med Genet.* 1991;28:443–447.
2. Neumann HP, Wiestler OD. Clustering of von Hippel-Lindau syndrome: evidence for a complex genetic locus. *Lancet.* 1991;337:1052–1054.
3. Wilding A, Ingham SL, Lalloo F, et al. Life expectancy in hereditary cancer predisposing diseases: an observational study. *J Med Genet.* 2012;49:264–269.
4. Lonser RR, Glenn GM, Walther M, et al. Von Hippel-Lindau disease. *Lancet.* 2003;361:2059–2067.
5. Binderup ML, Bisgaard ML, Harbud V, et al. Von Hippel-Lindau disease (vHL): national clinical guideline for diagnosis and surveillance in Denmark. 3rd ed. *Dan Med J* 2013;60:B4763.
6. Lonser RR, Butman JA, Huntoon K, et al. Prospective natural history study of central nervous system hemangioblastomas in von Hippel-Lindau disease. *J Neurosurg.* 2014;120:1055–1062.

7. Wanebo JE, Lonser RR, Glenn GM, Oldfield EH. The natural history of hemangioblastomas of the central nervous system in patients with von Hippel-Lindau disease. *J Neurosurg.* 2003;98:82–94.
8. Oosting SF, Brouwers AH, van Es SC, et al. ^{89}Zr-bevacizumab PET visualizes heterogeneous tracer accumulation in tumor lesions of renal cell carcinoma patients and differential effects of anti-angiogenic treatment. *J Nucl Med.* 2015;56: 63–69.
9. Gaykema SB, Brouwers AH, Lub-deHooge MN, et al. ^{89}Zr-bevacizumab PET imaging in primary breast cancer. *J Nucl Med.* 2013;54:1014–1018.
10. Loening AM, Gambhir SS. AMIDE: a free software tool for multimodality medical image analysis. *Mol Imaging.* 2003;2:131–137.
11. Oxnard GR, Zhao B, Sima CS, et al. Variability of lung tumor measurements on repeat computed tomography scans taken within 15 minutes. *J Clin Oncol.* 2011;29:3114–3119.
12. van Asselt SJ, Oosting SF, Brouwers AH, et al. Everolimus reduces ^{89}Zr-bevacizumab tumor uptake in patients with neuroendocrine tumors. *J Nucl Med.* 2014;55:1087–1092.
13. Takahashi A, Sasaki H, Kim SJ, et al. Markedly increased amounts of messenger RNAs for vascular endothelial growth factor and placental growth factor in renal cell carcinoma associated with angiogenesis. *Cancer Res.* 1994;54:4233–4237.
14. Wizigmann-Voos S, Breier G, Risau W, Plate KH. Up-regulation of vascular endothelial growth factor and its receptors in von Hippel-Lindau disease-associated and sporadic hemangioblastomas. *Cancer Res.* 1995;55:1358–1364.
15. Leung SY, Chan AS, Wong MP, Yuen ST, Fan YW, Chung LP. Expression of vascular endothelial growth factor in von Hippel-Lindau syndrome associated papillary cystadenoma of the epididymis. *Hum Pathol.* 1998;29:1322–1324.
16. Krieg M, Marti HH, Plate KH. Coexpression of erythropoietin and vascular endothelial growth factor in nervous system tumors associated with von Hippel-Lindau tumor suppressor gene loss of function. *Blood.* 1998;92:3388–3393.
17. Chan CC, Vortmeyer AO, Chew EY, et al. VHL gene deletion and enhanced VEGF gene expression detected in the stromal cells of retinal angioma. *Arch Ophthalmol.* 1999;117:625–630.
18. Miyagami M, Katayama Y, Nakamura S. Clinicopathological study of vascular endothelial growth factor (VEGF), p53, and proliferative potential in familial von Hippel-Lindau disease and sporadic hemangioblastomas. *Brain Tumor Pathol.* 2000;17:111–120.
19. de Vries EG, de Jong S, Gietema JA. Molecular imaging as a tool for drug development and trial design. *J Clin Oncol.* 2015;33:2585–2587.
20. Kumar VA, Knopp EA, Zagzag D. Magnetic resonance dynamic susceptibility-weighted contrast-enhanced perfusion imaging in the diagnosis of posterior fossa hemangioblastomas and pilocytic astrocytomas: initial results. *J Comput Assist Tomogr.* 2010;34:825–829.
21. Chen Y, Zhang J, Dai J, Feng X, Lu H, Zhou C. Angiogenesis of renal cell carcinoma: perfusion CT findings. *Abdom Imaging.* 2010;35:622–628.
22. Nagengast WB, Hooge MN, van Straten EM, et al. VEGF-SPECT with ^{111}In-bevacizumab in stage III/IV melanoma patients. *Eur J Cancer.* 2011;47:1595–1602.
23. Richard S, Gardie B, Couvé S, Gad S. Von Hippel-Lindau: how a rare disease illuminates cancer biology. *Semin Cancer Biol.* 2013;23:26–37.
24. Champion KJ, Guinea M, Dammai V, Hsu T. Endothelial function of von Hippel-Lindau tumor suppressor gene: control of fibroblast growth factor receptor signaling. *Cancer Res.* 2008;68:4649–4657.
25. Fisher R, Horswell S, Rowan A, et al. Development of synchronous VHL syndrome tumors reveals contingencies and constraints to tumor evolution. *Genome Biol.* 2014;15:433.
26. Shankar GM, Taylor-Weiner A, Lelic N, et al. Sporadic hemangioblastomas are characterized by cryptic *VHL* inactivation. *Acta Neuropathol Commun.* 2014;2: 167.
27. Liang X, Shen D, Huang Y, et al. Molecular pathology and CXCR4 expression in surgically excised retinal hemangioblastomas associated with von Hippel-Lindau disease. *Ophthalmology.* 2007;114:147–156.
28. Rioux-Leclercq N, Fergelot P, Zerrouki S, et al. Plasma level and tissue expression of vascular endothelial growth factor in renal cell carcinoma: a prospective study of 50 cases. *Hum Pathol.* 2007;38:1489–1495.
29. Los M, Aarsman CJM, Terpstra L, et al. Elevated ocular levels of vascular endothelial growth factor in patients with von Hippel-Lindau disease. *Ann Oncol.* 1997;8:1015–1022.
30. Thoma CR, Frew IJ, Hoerner CR, Montani M, Moch H, Krek W. pVHL and GSK3β are components of a primary cilum-maintanance signaling network. *Nat Cell Biol.* 2007;9:588–595.
31. Park JE, Keller GA, Ferrara N. The vascular endothelial growth factor (VEGF) isoforms: differential deposition into the subepithelial extracellular matrix and bioactivity of extracellular matrix-bound VEGF. *Mol Biol Cell.* 1993;4:1317–1326.
32. Wackernagel W, Lackner EM, Pilz S, Mayer C, Stepan V. Von Hippel-Lindau disease: treatment of retinal hemangioblastomas by targeted therapy with systemic bevacizumab. *Acta Ophthalmol.* 2010;88:e271–e272.
33. Omar AI. Bevacizumab for the treatment of surgically unresectable cervical cord hemangioblastoma: a case report. *J Med Case Rep.* 2012;6:238.
34. Riklin C, Seystahl K, Hofer S, Happold C, Winterhalder R, Weller M. Antiangiogenic treatment for multiple CNS hemangioblastomas. *Onkologie.* 2012;35: 443–445.
35. Piribauer M, Czech T, Dieckmann K, et al. Stabilization of a progressive hemangioblastoma under treatment with thalidomide. *J Neurooncol.* 2004;66:295–299.
36. Sardi I, Sanzo M, Giordano F, et al. Monotherapy with thalidomide for treatment of spinal cord hemangioblastoma in a patient with von Hippel-Lindau disease. *Pediatr Blood Cancer.* 2009;53:464–467.
37. Madhusudan S, Deplanque G, Braybrooke JP, et al. Antiangiogenic therapy for von Hippel-Lindau disease. *JAMA.* 2004;291:943–944.
38. Schuch G, de Wit M, Höltje J, et al. Case 2: hemangioblastomas—diagnosis of von Hippel-Lindau disease and antiangiogenic treatment with SU5416. *J Clin Oncol.* 2005;23:3624–3626.
39. Jimenez C, Cabanillas ME, Santarpia L, et al. Use of tyrosine kinase inhibitor sunitinib in a patient with von Hippel-Lindau disease: targeting angiogenic factors in pheochromocytoma and other von Hippel-Lindau disease-related tumors. *J Clin Endocrinol Metab.* 2009;94:386–391.
40. Jonasch E, McCutcheon IE, Waguespack SG, et al. Pilot trial of sunitinib therapy in patients with von Hippel-Lindau disease. *Ann Oncol.* 2011;22:2661–2666.
41. Roma A, Maruzzo M, Basso U, et al. First-line sunitinib in patients with renal cell carcinoma (RCC) in von Hippel-Lindau (VHL) disease: clinical outcome and patterns of radiological response. *Fam Cancer.* 2015;14:309–316.
42. Kim BY, Jonasch E, McCutcheon IE. Pazopanib therapy for cerebellar hemangioblastomas in von Hippel-Lindau disease: case report. *Target Oncol.* 2012;7: 145–149.